ELSEVIER

Journal of Nuclear Materials 277 (2000) 1–10

journal of nuclear materials

www.elsevier.nl/locate/jnucmat

Study of boron carbide evolution under neutron irradiation by Raman spectroscopy

D. Simeone[a,*], C. Mallet[a], P. Dubuisson[a], G. Baldinozzi[b], C Gervais[c], J. Maquet[c]

[a] *Laboratoire d'Etude des Matériaux Absorbants, CEA, CE Saclay, F-91191, Gif-sur-Yvette cedex, France*
[b] *Laboratoire de Chimie Physique du Solide, URA CNRS 453, Ecole Centrale Paris, F-92295 Châtenay-Malabry cedex, France*
[c] *Laboratoire de Chimie du Solide, URA CNRS 453, Ecole Centrale Paris, F-92295 Châtenay-Malabry cedex, France*

Received 26 March 1999; accepted 23 June 1999

Abstract

Boron carbide, $B_{12}C_3$, is an absorbing material used to control the reactivity of nuclear reactors by taking advantage of nuclear reactions (e.g. $^{10}B(n,\alpha)^7Li$), where neutrons are absorbed. During such reactions, radiation damages originating both from these nuclear reactions and from elastic collisions between neutrons and atoms lead to a partial destruction of this material, which gives the main limitation of its lifetime in nuclear reactors. In order to understand the evolution of $B_{12}C_3$ in nuclear plants, the effect of neutron irradiation in $B_{12}C_3$ has been investigated by Raman and nuclear magnetic resonance (NMR) spectroscopies. Comparisons of $B_{12}C_3$ samples irradiated by 1 MeV electrons, 180 keV helium ions and neutrons are used to study the microstructure evolution of this material by Raman scattering. The analysis of Raman spectra of different $B_{12}C_3$ samples irradiated by neutrons clearly shows that during the cascade displacements, the 485 and 527 cm^{-1} modes disappear. These characteristic features of Raman spectra of the neutron irradiated samples are interpreted by a microscopic model. This model assumes that the CBC linear chain is destroyed whereas icosahedra are self-healed. ^{10}B atoms destroyed during the neutron irradiation are replaced in icosahedra by other boron and carbon atoms coming from the linear CBC chain. The ^{11}B NMR analysis performed on unirradiated and irradiated B_4C samples shows the vanishing of a strong quadrupolar interaction associated to the CBC chain during the high neutron irradiation. The ^{11}B NMR spectroscopy confirms the previous Raman spectroscopy and the proposed microscopic model of $B_{12}C_3$ evolution under neutron irradiation.

1. Introduction

Over the last years, much work has been devoted to experimental and theoretical study of structural modifications occurring in some boron-rich compounds, which present unusual bondings and transport properties. One of the common features of boron-rich solids is the molecular-like structure based on 12 boron atoms icosahedra bonded to the neighboring icosahedra or to other elements belonging to the structure [1]. The nature of these bonds in the icosahedra and between other atoms depends on the particular elements included in the structure. The hardness and the refractory nature of the materials based on the structure of α-boron are due to strong bonds in a network of linked icosahedra. The main structure of $B_{12}C_3$ is trigonal; it consists of a molecular-like sub-unit based on 12 atoms forming an icosahedron located at the origin of the primitive trigonal cell and a linear chain of three atoms extending along the threefold axis formed by the CBC linear chain. The existence of a threefold axis and of an inversion center at the origin requires two independent atoms to describe the icosahedron. It is therefore possible to distinguish between six equatorial sites (forming bonds with the linear chain) and six polar sites (forming bonds with the neighboring icosahedra). In $B_{12}C_3$, 11 of the atoms constituting the icosahedron are boron, the remaining one being a carbon. A boron atom sits in the middle of the linear chain. The distribution of boron and

* Corresponding author. Tel.: +33-1 69 08 29 20; fax: +33-1 69 08 90 82.
E-mail address: dsimeone@cea.fr (D. Simeone).

0022-3115/00/$ - see front matter
PII: S0022-3115(99)00149-X

carbon atoms onto the different sites has been an active subject of debate but it is now admitted that the carbon atom in the icosahedron sits on a polar site [2]. Fig. 1 presents a schematic diagram of the boron carbide structure. The h1 sites refer to equatorial atoms (boron or carbon atoms), the h2 sites refer to polar atoms (boron atoms), Cc1 and Cc2 refer to carbon atoms of the threefold axis and Cb refers to the inversion center (boron atom).

X-ray scattering [2], Raman and infra-red spectroscopies [3–5], as well as nuclear magnetic resonance (NMR) [6] point out that the outstanding properties of $B_{12}C_3$ are related to its particular static and dynamic structural features.

This material is extensively used to control nuclear plants. Indeed, ^{10}B atoms can efficiently absorb low neutrons (with a kinetic energy of 0.025 eV) and fast neutrons (with a kinetic energy above 1 MeV). Moreover, its low fabrication cost, high melting point (2673 K) and low neutron activity make this material very attractive for the nuclear industry. However, the evolution of such a material under neutron irradiation is not well understood. In addition to damages produced by elastic collisions between neutrons and target atoms, the neutron capture reaction $^{10}B(n,\alpha)^7Li$ generates helium and lithium atoms with an average kinetic energy of 1.48 and 0.83 MeV, respectively. All these damages may induce point defects in $B_{12}C_3$. The knowledge of these point defects constitutes the aim of this paper.

In this work, we take advantage of the local sensitivity of the Raman scattering technique to localize the point defects in boron carbide that are produced at different neutrons fluences. The comparison between the experimental frequencies and those simulated by lattice dynamic calculation leads us to propose a model for the defective structure of this material. The ^{11}B NMR technique has been used to confirm the structural evolution of $B_{12}C_3$ under neutron irradiation.

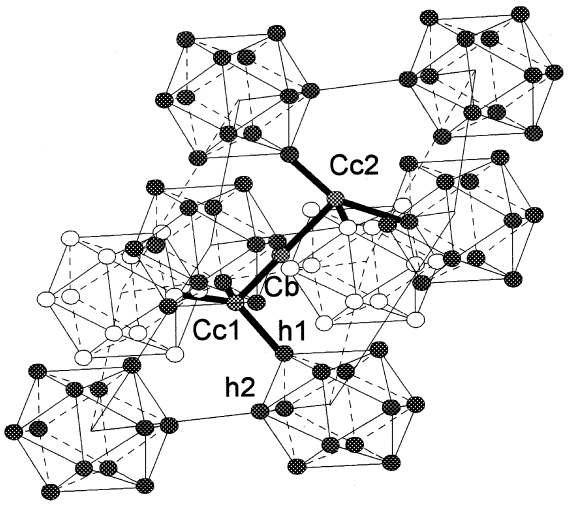

Fig. 1. Crystal structure of stochiometric $B_{12}C_3$. The inversion center (Cb) carbon sites (Cc), polar (h2) and equatorial sites (h1) in icosahedron are shown.

2. Experimental procedure

2.1. Sample preparation

Boron carbide polycrystalline samples including 19.8, 48 and 90 at.% of ^{10}B were prepared under hot pressing boron of carbide powder. After sintering, the samples are cylinders of 3.35 mm radius and of 2 mm high, formed of grains of about 10 μm size with a porosity of 4%. To assess the quality of the sintered samples, X-ray diffraction experiments were carried out on an Inel X-ray diffractometer equipped with a position sensitive detector using a monochromatic copper radiation. The lattice parameters of different samples were found to be in agreement with the expected stoichiometry. Chemical investigation by inductively coupled plasma analysis revealed the presence of Si (640 ppm (weight)), Fe (590 ppm (weight)), Al (200 ppm (weight)) and Mg (155 ppm (weight)).

Raman spectra were recorded by a T64000 triple monochromator spectrometer using a 300 mW argon-laser light at 514.5 nm and slit widths of 2 cm^{-1}. The beam spot was a 2 μm^2 circle and the scan time was 120 s per spectrum. All the spectra were obtained in accumulating five scans.

The ^{11}B NMR spectra were performed at 96.216 MHz on a Bruker MSL300 spectrometer. The static and magic angle spinning (MAS) spectra were recorded using a CP-MAS Doty probe with no probe background, equipped with 5 mm Si_3N_4 rotors. A $\pi/2$–τ–$\pi/2$ echo sequence was used for the static spectra in order to record the whole signal ($\tau = 100$ μs). For the MAS spectra, the spinning speed was set to 9 kHz. A recycle delay of 3 s was chosen according to the value of spin–lattice relaxation time T_1 measured ($T_1 = 600$ ms). The spectra were referenced externally to $BF_3 \cdot OEt_2$ at 0 ppm.

The ^{11}B MQ-MAS spectra have been acquired with 4 mm ZrO_2 rotors spinning at 13 kHz. A two-pulse hypercomplex sequence [7] with triple-quantum excitation and conversion pulses of 8 and 3 μs (for a radio frequency field strength of 83 kHz) was used with 73 and 33 μs increments for t_1 and t_2 dimensions, respectively. The recycle delay was set to 3 s and 792 scans were accumulated. The spectra were then processed according to a procedure very similar to that described for DAS [8].

2.2. Sample irradiation

Three different types of irradiation were performed for Raman scattering.

Under an electron beam: samples were irradiated at 323 K by a flux of 5.8×10^{18} cm^{-2} s^{-1} electrons with 1 MeV energy during 26 100 s.

Under a He^+ beam: samples were irradiated at room temperature by a flux of 10^{12} cm^{-2} s^{-1} He^+ ions with 180 keV energy during 9360 s.

Under neutrons: $B_{12}C_3$ cylinders were irradiated in a Pressurized Water Reactor (PWR) during 323 days by a neutron fluence of 3×10^{20} cm^{-2} at about 600 K.

The boron carbide samples analyzed in this paper contain 19.8 at.% of ^{10}B atoms in which neutrons from a PWR induce $^{10}B(n,\alpha)^7Li$ reactions. For neutrons with kinetic energies up to 20 MeV in PWRs, the capture cross section of this reaction can be described by a classical absorption law proportional to $AE^{-1/2}$, where E is the kinetic energy. The high value of A (3890 barn for neutrons with a kinetic energy of 0.025 eV) leads to an important self-shielding [9] of irradiated samples in PWRs. The low mean free path of thermal neutrons (1.85×10^{-5} m) and the high mean free path of fast neutrons (0.11 m) induce a steep decrease of the neutron flux as a function of the $B_{12}C_3$ pellets radius in PWRs. This neutron depletion inside $B_{12}C_3$ induces structural modifications in pellets as a function of the radius, which will be further studied in detail using a Raman microprobe. The changes observed in the Raman spectra only depend on the pellet radius, as it is shown by the spectra collected at different positions for given distances from the center of the cylinders.

3. Results and discussion

3.1. Raman scattering, spectra and assignment

The investigation of the Raman spectra of boron carbide gives valuable information about the crystal structure and its modifications and distortions. The number of lattice vibrations is well known from group theoretical investigations if no ordering of the carbon atom in the icosahedron occurs. The normal modes of vibration of the $B_{12}C_3$ compounds at the Brillouin zone center can be classified according to the following irreducible representations:

$$\Gamma(\mathbf{k}=0) = 5A_{1g} \oplus 2A_{2g} \oplus 7E_g \oplus 2A_{1u} \oplus 6A_{2u} \oplus 8E_u.$$

The A_{1g} modes are characterized by the central atom of the linear chain when it is at rest. The two terminal atoms of the chain vibrate along the threefold axis generating a symmetric stretching of the bonds. The vibration of the atoms in the icosahedra is rather general. The E_g modes are doubly degenerated symmetric stretching modes, rather similar to those belonging to the A_{1g} irreducible representation. The A_{2g} modes are not optically active: the atoms in the linear chain are at rest while the displacements of the atoms in the icosahedron are contained in the mirror.

This decomposition also includes odd modes. The A_{1u} modes are not infra-red active and are very close to those belonging to the A_{2g} irreducible representation. The A_{2u} modes are characterized by the central atom of the linear chain vibrating along the threefold axis and giving rise to an asymmetric stretching of the bonds with the terminal atoms of the chain. The E_u modes are doubly degenerated asymmetric stretching modes in which all atoms vibrate. Finally, one of the E_u modes and one of the A_{2u} modes have zero frequency and they represent the zone center's acoustic modes. The assignment of the peaks in the spectra to the motion of the atoms was qualitatively possible for $B_{12}C_3$ [10,11].

3.2. Model of force constants

3.2.1. Parameters of the model

$B_{12}C_3$ presents a molecular-like structure based on 12 atoms icosahedra bonded to the neighboring icosahedra (Table 1) and to a linear chain of three atoms (Fig. 1). The crystal stability comes from short range overlap interactions. The short range interaction energy is assumed to be the sum of two-bodies axially symmetric interactions limited to the neighbors. The electrostatic long range interaction has been neglected, since the ionic character of the bonds is very weak. Although $B_{12}C_3$ is composed of light elements, the study of its thermal expansion and thermal conductivity shows that anharmonic effects do not play an important part in the lattice potential energy used to describe lattice vibrations. As bonds between atoms in $B_{12}C_3$ are essentially covalent, the model used to calculate lattice vibrations is a Valence Force Field type.

The forces between atoms are governed by the electronic structure of the atoms involved. For the study of $B_{12}C_3$ vibrations, we have not tried to derive force constants of boron and carbon atoms from principles based on electronic waves function calculations. The

Table 1
Positions of the atoms in $B_{12}C_3$ in rhombohedral notation

Atom	Sites	x	y	z
Boron	Cb (chain)	0.0000	0.0000	0.5000
Carbon	Cc (chain)	0.0000	0.0000	0.3823
Boron	h1	0.3256	0.1628	0.3584
Boron	h2	0.2148	0.0107	0.1138

potential energy is expressed in terms of changes in bond distances.

Tersoff [12] has developed a semi-empirical model to describe highly oriented bonds in boron and carbon compounds. We tried to use a semi-empirical Tersoff-like potential for B and C by using the Tersoff's rule for multicomponent systems to model covalent bonds in $B_{12}C_3$. However, no accurate potential was found to reproduce the experimental cohesive energy of the crystal.

An empirical approach has been used to determine force constants. We do not attempt any exhaustive survey of the best fit. In fact, we scan realistic conditions based on physical grounds to find a correct set of parameters describing lattice vibration modes using the Valence Force Field. We only discuss a phenomenological approach based on the Valence Force Field often used for covalent atoms.

For each type of short range interactions, two parameters are needed to specify the axially symmetric forces. These parameters were chosen to be the second derivative of the short range potential V_i, parallel and perpendicular to the line joining the interacting atoms:

$$A_{ij} = \frac{2V}{e^2}\left(\frac{\partial^2 V_i}{\partial r_{ij}^2}\right),$$

$$B_{ij} = \frac{2V}{e^2}\left(\frac{1}{r_{ij}}\frac{\partial V_i}{\partial r_{ij}}\right).$$

In these relations, V is the volume of the unit cell, e is the electron charge and r_{ij} is the distance between atoms i and j.

The usual determination of these coefficients is obtained by fitting the experimental phonons dispersion curves. Unfortunately, no inelastic neutron scattering on a triple axis spectrometer can be performed in the present case, as we do not dispose of boron carbide enriched in ^{11}B single crystals to avoid the very strong absorption cross section of thermal neutrons of ^{10}B. For these reasons, coefficients A_{ij} and B_{ij} were calculated directly by fixing the infra-red frequency values and by refining them to obtain the best fit of the Raman frequencies.

3.2.2. Study of force constants

Some hypotheses have been made to calculate the 14 parameters A_{ij} and B_{ij} used in the lattice vibration calculation.

- The highest infra-red and Raman modes were experimentally found to be A_{2u} (1560 cm^{-1}) and A_{1g} (1060 cm^{-1}) modes. These modes impose values for Cb–Cc force constants.
- Inside icosahedra, h1–h1 and h1–h2 bonds have the same lengths and are quite equivalent. For this reason, we impose the equality of force constants for these bonds.
- The infra-red frequencies measured by Bouchacourt [13] on different samples (with a 20 at.% of carbon) have been used to estimate force constants.
- To complete the fit, we impose two inequalities. Firstly, to take into account the compression of icosahedron observed in compression experiments [14], the force constants A_{h1-h1} and A_{h2-h2}^{intra} must be less important than A_{h1-Cc} and A_{h2-h2}^{inter} force constants. Secondly, we impose upon the A_{h1-h1} and A_{h1-h2} force constants to be inferior to the value of A_{h2-h2}. This condition can be understood as follows: equatorial sites (h1) are linked with carbon atoms of the linear chain. This bond needs electrons and fewer electrons are available for intra-icosahedron bonds than for polar atoms (h2).

A set of four parameters permits all these relations to be satisfied. The numerical values of force constants are listed in Table 2. Table 3 presents the comparison between experimental [14,15] and calculated Raman and infra-red modes in $B_{12}C_3$.

The principal interest of this calculation is to show that 480 and 530 cm^{-1} vibration modes are associated with the CBC chain vibrations. Eigenvectors associated with these two modes belong to the E_g irreducible representation. The modes above 600 cm^{-1} are mainly related to internal vibrations of the icosahedra, in agreement with previous investigations [15]. Moreover, the model permits the average sound velocity of the material to be calculated. The comparison between the calculated value (9.1 km/s) and the measured one (9.5 km/s [16]) is quite good. As expected, the analysis of force constants shows that mechanical properties of $B_{12}C_3$ (high Young's modulus...) are essentially due to the linear CBC chain. The fit gives positive values of B_{ij} constants, that are inferior to a tenth of the A_{ij} values, as it is the case in ionic materials. The simple rule saying that the force constant A_{ij} decreases as the bond length increases is observed excepted for the Cc–h1 bond. The carbon atom of the linear chain seems to reinforce the covalent bond of the CBC chain, which weakens Cc–h1 bonds. The relatively high value of A_{Cb-Cc} is not surprising. The bonding of the central linear CBC chain is

Table 2
Bond lengths in Å [10], radial A_{ij} and tangential B_{ij} force constants between neighbors in $B_{12}C_3$

Sites	A_{ij}	B_{ij}	Bond lengths (Å)
Cb–Cc	6.72	0.7920	1.429
Cc–h1	0.74	0.0264	1.617
h2–h2 (inter-icosahedra)	2.55	0.0024	1.732
h2–h2	1.99	0.0720	1.821
h2–h1	0.72	0.0720	1.796
h1–h2	0.72	0.0072	1.796
h1–h1	0.70	0.0744	1.773

Table 3
Observed and calculated Raman frequencies for unirradiated $B_{12}C_3$ at room temperature

Mode	Calculated frequencies by VFF (cm^{-1})	R.I.	Experimental frequencies (cm^{-1})
01	1557	A_{2u}	1560
02	1111	A_{1g}	1060
03	952	E_g	998
04	952	E_g	998
05	902	A_{1u}	?
06	900	A_{1g}	938
07	721	E_u	952
08	721	E_u	952
09	682	E_g	845
10	682	E_g	845
11	640	A_{2u}	840
12	656	E_u	694
13	656	E_u	694
14	586	A_{2u}	?
15	582	A_{1g}	813
16	574	E_g	780
17	574	E_g	780
18	575	E_u	578
19	575	E_u	578
20	**521**	**E_g**	**527**
21	**521**	**E_g**	**527**
22	509	A_{1g}	?
23	**487**	**E_g**	**480**
24	**487**	**E_g**	**480**
25	464	A_{2u}	?
26	460	A_{1g}	374
27	462	A_{2g}	?
28	461	E_u	?
29	461	E_u	?
30	394	E_u	394
31	394	E_u	394
32	375	E_g	330
33	375	E_g	330
34	368	A_{2g}	?
35	307	E_u	?
36	307	E_u	?
37	255	E_u	?
38	255	E_u	?
39	170	A_{1u}	168
40	167	Eg	?
41	167	Eg	?
42	109	A_{2u}	?
43	0	A_{2u}	
44	0	E_u	
45	0	E_u	

characterized by a strong covalent bond. In the range of frequencies from 600 to 1000 cm^{-1}, calculated and experimental frequencies disagree, whereas for some frequencies expected to be due to the CBC chains, calculated and observed frequencies agree quite well. A possible explanation for these facts may be found in the potential energy description used. Such a model does not take into account second neighbor's interactions, which may stabilize the icosahedron.

3.2.3. Comparison between α-boron and $B_{12}C_3$

A comparison of α-boron and boron carbide spectra with different carbon concentrations is reported by Tallant et al. [15]. The main structural difference between α-boron and boron carbide is due to the linear CBC chain that is present in the latter compound. We conclude that the two narrow peaks at 485 and 527 cm^{-1} are related to the existence of this CBC chain. The Raman spectrum of $B_{12}C_3$ containing 20 at.% of carbon displays relatively broad bands in the region above 600 cm^{-1}. The broadening of these peaks may be due to the substitutional disorder induced by the replacement of boron atoms by carbon atoms in the icosahedra.

3.3. Effects produced by irradiation

Different samples of $B_{12}C_3$ have been irradiated by electrons, He^+ and neutrons. To compare the effects of these three types of irradiations, different samples are classified according to their displacements per atoms (dpa) values. The dpa is a crude estimation of the effective damages induced by the different kinds of radiations in the material [9].

3.3.1. Electron irradiation

The dpa induced by the electron beam in the $B_{12}C_3$ was calculated by the Lesueur method [17] using the relativistic electron–atom cross section derived by Mott [18]. The threshold energy used in calculations was 20 eV for both atoms. The Raman spectra of $B_{12}C_3$ irradiated by electrons at 2.8 dpa values is similar to the unirradiated $B_{12}C_3$ Raman spectrum (Fig. 2).

3.3.2. He^+ irradiation

The implantation curve of 180 keV He^+ ions versus the penetration depth in the $B_{12}C_3$ samples was calculated by the Transport Ions in Matter (TRIM) code which uses the Ziegler's formalism [19]. The average implantation depth of He^+ in $B_{12}C_3$ is close to 0.6 μm. The atomic concentration of He atoms in the samples may be considered to be constant and equal to 10^{-3} at 1 dpa and to 2×10^{-3} at 2 dpa. The Raman spectra of $B_{12}C_3$ samples corresponding to these situations are presented in Fig. 3. The intensities of the two narrow peaks at 485 and 527 cm^{-1} decrease when the dpa increases. A new broad peak near 155 cm^{-1} appears for dpa values above 1 dpa. In a further step, the most irradiated samples were annealed at 773 K during 30 min. A comparison of Raman spectra collected before and after the annealing (Fig. 4) unambiguously shows that these two peaks are restored. The calculated diffusion length of He atoms in non irradiated $B_{12}C_3$ samples [20] is 53 Å. This value being noticeably smaller than the

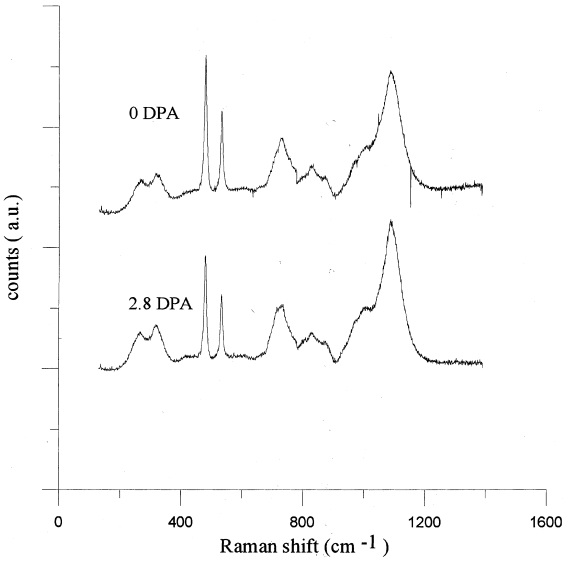

Fig. 2. Comparison between electron irradiated Raman spectra and unirradiated $B_{12}C_3$.

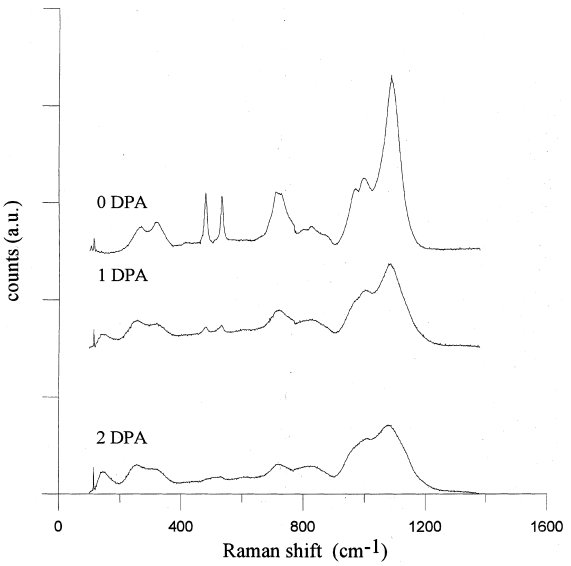

Fig. 3. Comparison between He^+ irradiated Raman spectra and unirradiated $B_{12}C_3$.

sample size (0.2 mm), the diffusion of He atoms in the sample can be neglected. Therefore the difference observed on the annealed and initial implanted He^+ Raman spectra cannot be due to a possible helium diffusion out of the implanted sample during the annealing. One increasing the annealing temperatures, the 155 cm^{-1} broad peak vanishes whereas the 485 and 527 cm^{-1} peaks appear.

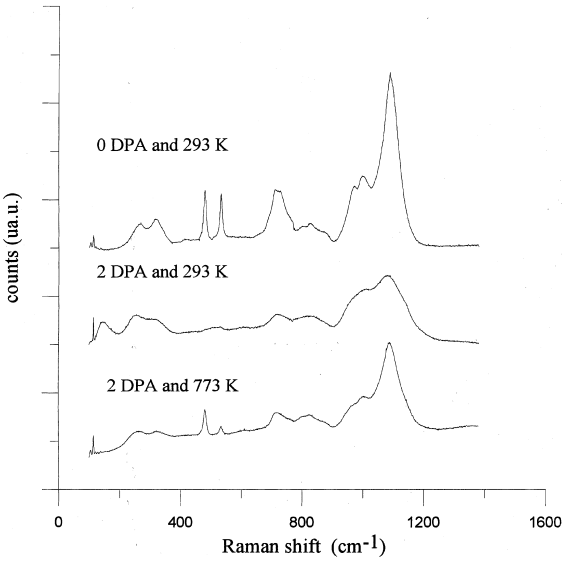

Fig. 4. Effect of an annealing at 773 K for 30 min of $B_{12}C_3$ irradiated by He^+ ions.

3.3.3. Neutron irradiation

In addition to the damages produced by the elastic scattering between neutrons and target nuclei, the inelastic scattering is a further source of damage: indeed, ^{10}B nuclei are strong neutron absorbers according to the $^{10}B(n,\alpha)^7Li$ reaction. He and Li atoms, which possess an average kinetic energy of 1.48 and 0.83 MeV respectively, are produced in irradiated samples. The absorption process of neutrons by ^{10}B atoms leads to a modification of the dpa profile versus the cylinder radius [9]. Fig. 5 presents Raman spectra of neutron irradiated $B_{12}C_3$ samples with different numbers of dpa. They are similar to those already displayed in Fig. 3. Moreover, the 155 cm^{-1} broaden peak appears also for values of about 1 dpa and vanishes for high dpa values (about 15 dpa). Fig. 6 presents the evolution of Raman spectra of irradiated B_4C samples at 2 dpa by neutrons and annealed at different temperatures. No restoration of the 480 and 527 cm^{-1} peaks occurs.

4. Possible healing mechanisms in $B_{12}C_3$

During the scattering process under 1.2 MeV electrons flux, recoil atoms acquire enough energy (470 and 520 eV for B and C atoms, respectively) to break bonds. But cascades induced by these atoms are not as dense as those induced by 180 keV He^+ implantation or neutrons irradiation. In this process, the target atom is knocked out with its core electrons (but it will stay very close to the initial position). It will leave its site with a net positive charge and its valence electrons will be redistributed

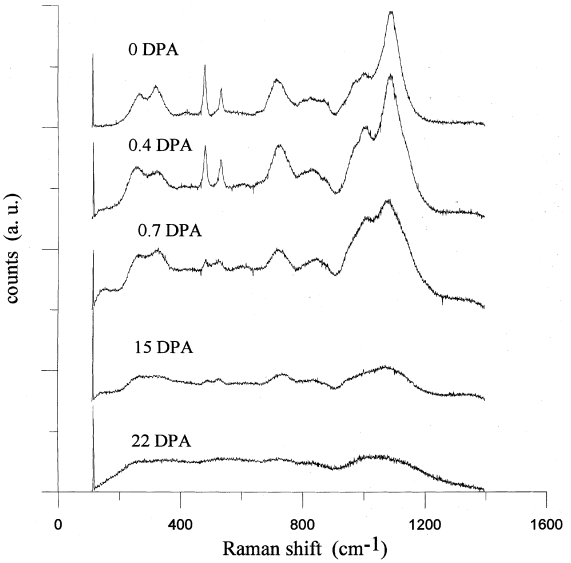

Fig. 5. Comparison between neutron irradiated Raman spectra and unirradiated $B_{12}C_3$.

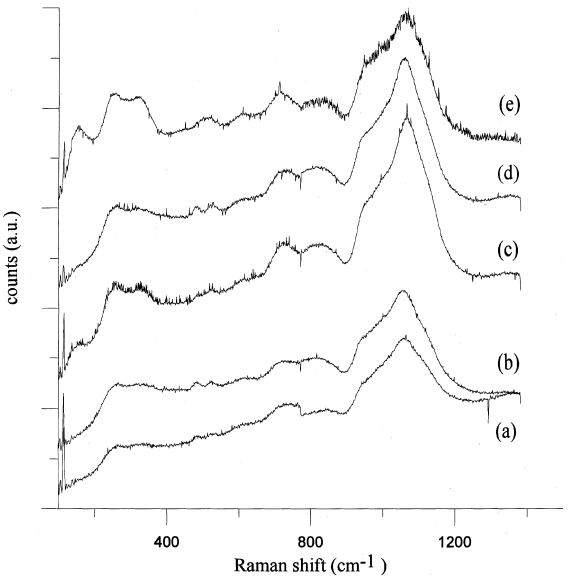

Fig. 6. Effect of different annealings of $B_{12}C_3$ irradiated by neutrons: (a) unannealed irradiated by neutrons at 2 dpa sample; (b) annealed sample 30 min at 373 K; (c) annealed sample 30 min at 573 K; (d) annealed sample 30 min at 673 K; (e) annealed sample 30 min at 373 K.

among the nearest neighbors. This situation of a positive charged ion occupying an interstitial position in a negative charged environment is highly unstable and the atom will soon relax to the original configuration. Therefore, a self-healing mechanism will take place for this kind of irradiation [21].

The He^+ and neutron scattering pictures are rather different. Thermal neutrons are responsible for the $^{10}B(n,\alpha)^7Li$ reactions producing atoms having high kinetic energies. These atoms produce displacement cascades. The same considerations hold for fast neutrons having a kinetic energy higher than 1 MeV and for 180 keV He^+ irradiations. During these scattering processes, the displacement cascades will destroy both the linear chain and the icosahedra, and the kicked atoms will move in the material far from the impact position. Nevertheless, the situation of the atoms in the linear chain is quite different from that of the atom in the icosahedron. In fact, when one atom among 12 in the icosahedron is kicked out, it is reasonable to suppose that the icosahedron, though very perturbed, will survive after the shock. The residual part of the icosahedron will try to restore its original configuration and in order to do that, it captures one of the atoms of the neighboring linear chain. Therefore, the icosahedra will self-heal, as in the case of electron scattering. If one of the three atoms is kicked out of a linear chain, no process of this kind can be invoked. Therefore, it is unlikely to have linear chains self-healing. A He^+ implantation does not modify the nature of knocked atoms. After the scattering, carbon and boron atoms forming the linear CBC chain stay in an interstitial position. Annealing permits atoms to relax in their original configuration. This explains the apparition of the 485 and 527 cm^{-1} peaks after the annealing. Neutron irradiation leads to the destruction of ^{10}B atoms. To self-heal, icosahedra pump interstitial atoms. At the end of the irradiation, no more atoms stay in an interstitial position and the annealing does not induce the restoration of the 485 and 527 cm^{-1} peaks. These mechanisms explain the behavior of the two 485 and 527 cm^{-1} peaks in Raman spectra.

This model may explain the evolution of the 155 cm^{-1} peak during He^+ and neutron irradiations. The possible transformation of linear CBC chains into CBB or BBB chains during irradiation cannot explain such a peak because the weak force constants (and then the high length of the C–B or B–B bond) necessary to explain such a peak do not seem realistic. Another possible explanation is to suppose that such a peak is associated with disorder induced by irradiation. This disorder is correlated to dpa and should not vanish when the dpa increases. This disagrees with experimental spectra (Fig. 5). The model of $B_{12}C_3$ evolution under irradiation shows that $B_{12}C_3$ evolves under irradiation to an α-boron-like structure. Then the 155 cm^{-1} may be associated with Δ (weak covalent bonds linking h2–h2 boron atoms in α-boron. These bonds ensure the cohesion of theα-boron structure) bond vibration. This explains why such a 155 cm^{-1} peak is also observed in Raman spectra of α-boron samples [16]. During a neutron irradiation, for high dpa values (about 15 dpa), many ^{10}B atoms are destroyed in icosahedra and replaced by carbon atoms

which do not allow the creation of Δ bonds. This analysis agrees with the experimental results of Fig. 5, which do not exhibit such a peak for high dpa values.

5. NMR studies of $B_{12}C_3$

5.1. NMR characterisation of $B_{12}C_3$

The ^{11}B static spectrum of the $B_{12}C_3$ is presented in Fig. 7(a). It shows a large signal around 0 ppm that can be assigned to the boron atoms in the icosahedra and a downfield shoulder attributed to the boron atoms in the linear chains [22]. To confirm this attribution, we decided to record the spectrum of a $B_{12}C_3$ sample 90% enriched in ^{10}B. Indeed, in that case, the number of ^{11}B atoms in the linear chains will decrease to 0.8 % and the corresponding signal should almost disappear. Moreover, this permits to decrease noticeably the homonuclear ^{11}B–^{11}B interaction in icosahedra partly responsible for the broadening of the signal and which can be estimated in a single ^{11}B–^{11}B pair as $\omega_d = 16$ kHz with a B–B distance of 1.7 Å [23]. Moreover, in the case of the icosahedra, it should be noted that the dipolar coupling of ^{11}B with 5 or 6 equivalent ^{11}B in the h1 and h2 sites, respectively must be considered. The ^{11}B static spectrum of the ^{10}B enriched $B_{12}C_3$ shown in Fig. 7(b) is indeed narrower and the lowfield shoulder has disappeared. The ^{11}B MAS spectrum of the same sample in which residual dipolar interaction are avereged by rotation shows many spinning sidebands (Fig. 7(c)) and a main signal between 10 and −15 ppm that seems to present at least two components (Fig. 7(d)). However, a precise identification of the various components is difficult due to the large overlap of the signals.

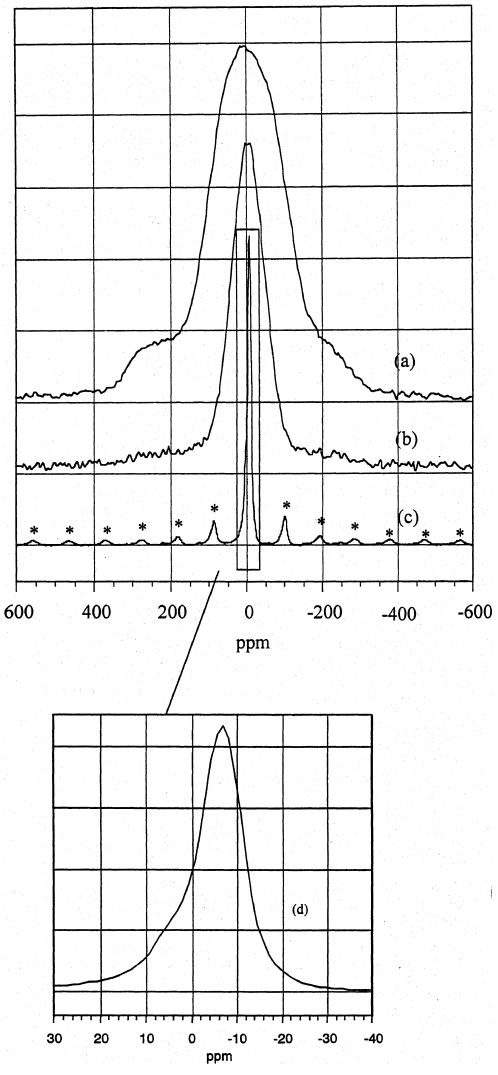

Fig. 7. ^{11}B static solid-state NMR experimental spectra of: (a) $B_{12}C_3$; (b) $B_{12}C_3$ enriched in ^{10}B; (c) ^{11}B MAS spectrum of $B_{12}C_3$ enriched in ^{10}B (Spinning rate = 9 kHz); (d) zoom of (c) between 30 and −40 ppm.

In order to improve the spectral resolution, we decided to use the 2D Multi-Quanta magic angle spinning (MQ-MAS) sequence: this experiment was recently proposed by Frydman and Harwood [24] who discovered that an isotropic spectrum of a quadrupolar nucleus broadened by second-order quadrupolar interaction could be obtained by a skew projection of a two-dimensional (triple quantum, single quantum) correlation spectrum. The 2D 3Q-MAS NMR spectrum of the ^{10}B enriched $B_{12}C_3$ is presented in Fig. 8 and shows the presence of two signals: one centered around −6 ppm with a rather large and symmetric 2D pattern, another one, narrower, that spreads in a direction parallel to the theoretical $\delta_{F1} = 17/8\delta_{F2}$ axis, which is characteristic of a large distribution of chemical shift values. A precise simulation of these signals is quite difficult, but they can be attributed to the h1 and h2 sites of the icosahedra corresponding to $\underline{B}B_5C$ and $\underline{B}B_6$ environments. We do not have enough information to assign without ambiguity the two signals to one or to the other site.

5.2. Effects produced by neutron irradiation

The $B_{12}C_3$ sample, composed of 48 at.% of ^{10}B atoms, has been irradiated in a fast Breeder Reactor (avoiding ^{10}B self-shielding effect) up to 250×10^{20} captures cm^{-3}. The ^{11}B static spectrum of the $B_{12}C_3$ after neutron irradiation is presented in Fig. 9(b). It shows a large signal around 0 ppm but the additional signal at lower field assigned to the boron atoms in the linear chains present in the unirradiated $B_{12}C_3$ (Fig. 9(a)) has disappeared, suggesting a removal of these chains. After annealing at 1200°C, the signal of the chains in the irradiated sample is still absent (Fig. 9(c)) which means that no evolution of the material appear during an-

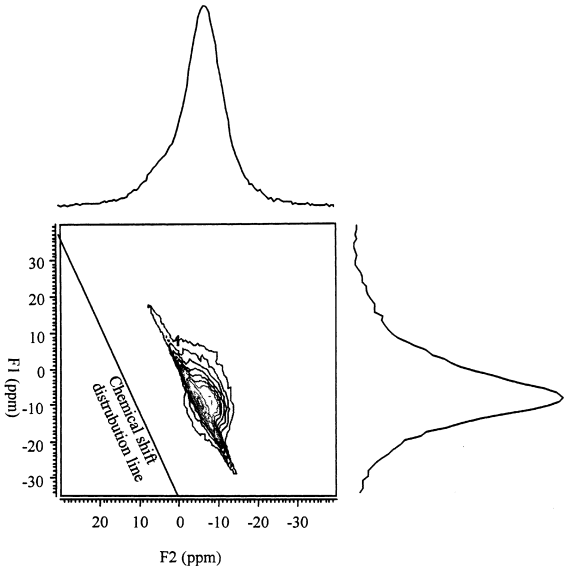

Fig. 8. ^{11}B 3Q-MAS NMR spectrum of the $B_{12}C_3$ sample enriched in ^{10}B.

nealing at high temperature. Moreover, the ^{11}B MAS NMR spectra of the $B_{12}C_3$ before and after irradiation are very similar (Fig. 10) and show the two signals characteristic of the boron sites in the icosahedra. This suggests that the icosahedric structures are maintained after irradiation in good agreement with the proposed healing mechanism. It is also interesting to notice, regarding the ^{11}B static spectra of the $B_{12}C_3$ before and after irradiation (Fig. 9) that the signals due to the boron atoms in the icosahedra in the irradiated samples are narrower. This could be due to the replacement of boron atoms kicked out of the icosahedra by neutrons, by carbon atoms of the C–B–C chains as suggested in the healing mechanism. Indeed, this would remove some ^{10}B–^{11}B interactions that broaden the spectra.

6. Conclusion

This work has extended previous studies of radiation damages in $B_{12}C_3$ [21] using a Raman microprobe to analyze the unit cell evolution of this material under different kinds of irradiations (electrons, He^+ ions and

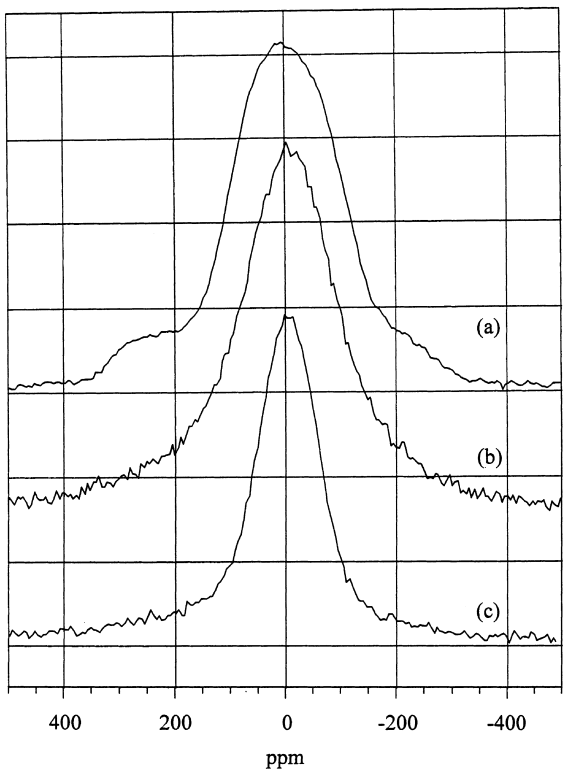

Fig. 9. ^{11}B static NMR spectra of: (a) $B_{12}C_3$; (b) $B_{12}C_3$ after irradiation; (c) $B_{12}C_3$ after irradiation and pyrolysis at 1200°C.

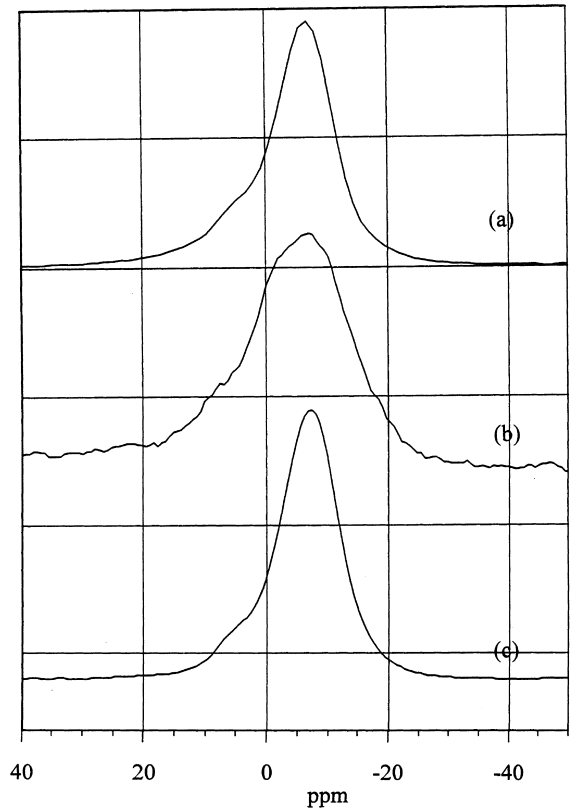

Fig. 10. ^{11}B MAS NMR spectra of: (a) $B_{12}C_3$ enriched in ^{10}B; (b) $B_{12}C_3$ after irradiation; (c) $B_{12}C_3$ after irradiation and annealed at 1473 K.

neutrons) [21,25]. Boron carbide form crystals comprising 12 atoms, boron-rich icosahedra, and linear, three atoms intericosahedral, chains. Using a classical Valence Force Field model for covalent structures, a set of force constants A_{ij} and B_{ij} have been fitted to simulate Raman frequencies of unirradiated B_4C samples. This set of force constants agrees with previous experimental works which associate 485 and 527 cm^{-1} peaks to the CBC linear chain vibrations. The absence of observed amorphisation or defect clusters in B_4C irradiated by electrons [24], and the observed disappearing of the CBC linear chain during neutron [26] and He^+ irradiation, lead us to confirm and to extend the model of $B_{12}C_3$'s self-healing under irradiation [21]. Different annealings of neutron and He^+ irradiated $B_{12}C_3$ samples, clearly show that:

- Under a He^+ irradiation, knocked atoms of the linear CBC chain stay in interstitial position in the unit cell. They relax in stable positions, reforming the CBC chain during the annealing.
- Under a neutron irradiation, some ^{10}B atoms of the icosahedra are destroyed and replaced by knocked atoms of the CBC chain. No more atoms exist in interstitial position, and an annealing does not allow to rebuild the CBC chain.

NMR spectra collected on irradiated and unirradiated $B_{12}C_3$ samples confirm the destruction of the CBC chain of B_4C under irradiation and the possible model proposed explaining the high stability of such a structure under neutron irradiation.

Acknowledgements

It is a pleasure to thank Dr D. Lesueur (CEA Saclay) for the helpful discussions during the various stages of this work.

References

[1] D. Emin, Phys. Today 1 (1987) 55.
[2] H. Yackel, Acta Crystallogr. B 31 (1975) 1797.
[3] M. Bouchacourt, F. Thevenot, J. Less Common Met. 82 (1981) 219.
[4] G. Will, K. Kossobutzki, J. Less Common Met. 44 (1976) 87.
[5] T. Aselage, D. Tallant, Phys. Rev. B 5 (1998) 2675.
[6] A. Silver, P. Bray, J. Chem. Phys. 31 (1959) 247.
[7] D. Massiot, B. Touzo, D. Trumeau, J.P. Coutures, J. Virlet, P. Florian, P.J. Grandinetti, Solid State NMR 6 (1996) 73.
[8] P.J. Grandinetti, J.H. Baltisberger, A. Llor, Y.K. Lee, U. Werner, M.A. Eastman, A. Pines, J. Magn. Res. A 103 (1993) 72.
[9] D. Simeone, O. Hablot, V. Micalet, P. Bellon, Y. Serruys, J. Nucl. Mater. 246 (1997) 206.
[10] C. Beckel, M. Youssaf, in: D. Emin, T. Aselage, C. Beckel, A. Switendick, B. Morosin (Eds.), Boron Rich Solids, Proceedings of the 10th International Symposium on Boron, Borides and Related Compounds, AIP Conference Proceedings, vol. 231, Am. Inst. of Phys., New York, 1991.
[11] K. Shirai, S. Emura, J. Phys.: Condens. Matter 8 (1996) 10991.
[12] J. Tersoff, Phys. Rev. B 8 (1989) 5566.
[13] M. Bouchacourt, thesis, I.N.P.G., France, 1982, p. 176.
[14] C. Beckel, M. Youssaf, in: D. Emin, T. Aselage, C. Beckel, A. Switendick, B. Morosin (Eds.), Boron Rich Solids, Proceedings of the 10th International Symposium on Boron, Borides and Related Compounds, AIP Conference Proceedings, vol. 231, Am. Inst. of Phys., New York, 1991.
[15] D. Tallant, T. Aselage, A. Campbell, D. Emin, Phys. Rev. B 8 (1989) 5649.
[16] P.Turkes, E. Swartz, R. Pohl, in: D. Emin, T. Aselage, C. Beckel, I. Howard, C. Wood (Eds.), Boron Rich Solids, Proceedings of International Symposium on Boron, Borides and Related Compounds, AIP Conference Proceedings, vol. 140, Am. Inst. of Phys., New York, 1986.
[17] D. Lesueur, Philos. Mag. A 44 (1981) 909.
[18] N. Mott, Proc. Roy. Soc. London A 125 (1932) 429.
[19] J. Ziegler, Handbook of Stopping Power of Energetic Ions in All Elements, 1980.
[20] J. Clayton, W. Bostom, Metals Ceramics and Materials, Report WAPD 255, 1962.
[21] H. Carrard, D. Emin, L. Zuppiroli, Phys. Rev. B 51 (1995) 11270.
[22] R.J. Kirkpatrick, T. Alesage, B.L. Philips, B. Montez, AIP Conf. Proc. 231 (1991) 261.
[23] L. Frydman, J.S. Harwood, J. Am. Chem. Soc. 117 (1995) 5367.
[24] H.K. Clark, J.L. Hoard, J. Am. Chem. Soc. 65 (1943) 2215.
[25] T. Stoto, J. Ardonceau, L. Zuppiroli, Radiat. Eff. 90 (1987) 17.
[26] C. Tucker, P. Senio, Acta Crystallogr. 8 (1955) 371.